American Mineralogist, Volume 60, pages 607–620, 1975

Mineralogy and Rare Earth Geochemistry of Apatite and Xenotime from the Gloserheia Granite Pegmatite, Froland, Southern Norway

REIDAR ÅMLI
Mineralogisk-Geologisk Museum, Sarsgt. 1, Oslo 5, Norway

Abstract

The Gloserheia granite pegmatite, situated in the Precambrian Kongsberg-Bamble formation, contains eight different zones (core, intermediate zones I-V, wall zone, and border zone). Apatite occurs in the core and in zones I and III. Xenotime has been found included in apatite from all three zones, and in other parageneses within these zones. The apatite close to xenotime inclusions is depleted in REE. Zoning of xenotime is characterized by an enrichment of the light REE relative to the heavy REE, from the center towards the rim of the crystal. Xenotime crystals included in apatite from the outer zones show less relative enrichment in the light REE than do those in the inner zones of the pegmatite. No such trend in REE fractionation is shown by xenotimes from other parageneses. The rare earth minerals included in apatite are considered to have formed by exsolution, possibly accompanied by metasomatism. Fractionation in the apatite-xenotime system was caused by processes bearing a simple relation to the crystallization of the zones where these minerals occur. In contrast, the REE fractionation in the other xenotimes probably has a more complex relation to the sequence of zones in the pegmatite.

Introduction

The Gloserheia granite pegmatite is situated in the Precambrian Kongsberg-Bamble formation, in Froland commune approximately 9 km N of Arendal (8°43′36″ E, 58°32′20″ N).

The pegmatite has been briefly described by Andersen (1926, 1931) and the geology of the Arendal-Gloserheia area by Bugge (1943). According to Bugge the rocks are of both granulite and amphibolite facies. Radiometric dating of rocks in the Arendal area has yielded ages from 850 to 1300 m.y.; ages for the pegmatites are from 875 to 1030 m.y. (Broch, 1963).

The pegmatite is V-shaped and exhibits in general a well developed and regular zoning. The following zones (Cameron *et al,* 1949) can be distinguished: core, intermediate zones I-V, wall zone, and border zone. Table 1 shows the mineral composition of the different zones.

This study concerns apatite and xenotime from different zones in the pegmatite, with special emphasis on rare earth geochemistry and the genesis of REE-bearing inclusions in apatite.

Apatite

Apatite is among the most abundant minor minerals in the pegmatite (Table 1), especially in intermediate zone I, where it is found as roughly equidimensional euhedral-to-subhedral crystals up to a size of one meter. Commonly well developed forms include a prism, pyramid (occasionally two sets), and basal pinacoid, and crystals are sometimes doubly terminated. The color is dominantly medium to dark green, but sometimes grayish to reddish.

In the core, apatite is much less common, medium to dark green in color, and generally smaller and better developed than in intermediate zone I. The crystal forms are the same. It is closely associated with microcline perthite and sporadically with 1*M* muscovite.

Apatite occurs in intermediate zone III as infrequent yellowish-green subhedral to anhedral crystals from a few mm to several cm in length. Very rarely, colorless euhedral crystals, several mm in size, are found embedded in calcite (all later discussion refers, however, to the first mentioned type).

In intermediate zone I, veins of colorless apatite—some with calcite, small amounts of hematite, and more rarely mm-sized xenotime crystals—cut the earlier apatite crystals, these veins presumably representing a late stage formation. It is not known if these "veins" extend outside the apatite.

All apatite from the Gloserheia pegmatite contains variable amounts of inclusions. Dissolution of 6.088

TABLE 1. Mineral Composition of the Different Zones in the Gloserheia Pegmatite

Mineral \ Thickness	Core	Int. zone I ½-3 m	Int. zone II 0.2-1 m	Int. zone III 10 cm	Int. zone IV 10 cm	Int. zone V 5-8 m	Wall zone 0.1-1.5m	Border zone 10 cm
Quartz	M	A	T	A	M	M	M	M
Microcline	T	M		A	A	M	A	
Plagioclase			M	M	M	A	M	M
Biotite		A		A	A	A	A	A
Muscovite		A	A/T	A/T	T(?)	T(?)	T(?)	T(?)
- " - 1 M	T							
Tourmaline	T	T		T				
Allanite		T		T				T
Apatite	T	T		T				
Euxenite				T				
Calcite		T	T	T				
Pyrite	T	T		T				
Magnetite		T					T	T
Rutile	T	T		T				
Xenotime	T	T		T				
Zircon				T				
Yttrotitanite				T				
Goethite	T	T		T				
Chlorite				T				
β-uranophane				T				
Uranophane				T				
Kasolite				T				
Fourmarierite				T				
Uraninite				T				
Thorite		T		T				
Beryl			T	T				
Monazite	T	T						
Hematite		T						

M: Main mineral
A: Accessory mineral
T: Trace mineral

kg of apatite from intermediate zone I in 6N HCl yielded 1.15 wt percent insoluble inclusions identified as xenotime, quartz, plagioclase (?), monazite, rutile, pyrite, and geothite. Their habit varies from euhedral to anhedral and from short prismatic to extremely long-prismatic (Fig. 1, I). Examination of apatite thin sections with electron microprobe (semi-quantitative) and optical microscope revealed, as additional inclusions, calcite (?) in apatite from the core and from intermediate zones I and III, and thorite in apatite from intermediate zone III.

Similar inclusions in apatites have been reported by several investigators. Taborszky (1962) has found zircon, hornblende, and mica oriented mostly parallel to the apatite *c* axis in the granitic to gabbroic rocks of the Odenwald province, West Germany. McKeown and Klemic (1957) observed monazite, bastnaesite, and hematite in apatite from the magnetite deposits at Mineville, New York; Pigorini and Veniale (1968) found monazite, xenotime, plagioclase (?), and biotite (the long prismatic inclusions oriented parallel to the apatite *c* axis) in the granitic to granodioritic rocks of the Val Sessera province, Italy.

Fractures in the Gloserheia apatites tend to be subparallel to prism or base in accordance with the reported parting for apatite (Tröger, 1959). Long-prismatic crystals crossing a fracture in the apatite showed no lateral displacement even on the μm scale.

Xenotime

Xenotime is the most abundant mineral found in the apatite from all zones. Examination by scanning electron microscope and polarizing microscope has revealed euhedral-to-anhedral and short-to-long prismatic xenotimes (Fig. 1, I-IV). When viewed with a binocular microscope (× 65), xenotime appears colorless or light yellow.

Studies with the universal stage show that all long prismatic xenotimes are oriented with their *c* axis parallel to the apatite *c* axis (as is true of long prismatic quartz crystals). Some inclusions (plagioclase ?) have axes of elongation parallel to the apatite *c* axis but show inclined extinction. Randomly oriented equidimensional inclusions (both quartz and xenotime) also occur. The long prismatic xenotimes occur throughout the crystals but tend to be concentrated along planes or lines (Fig. 1, VI). Equidimensional inclusions (mostly xenotime) also tend to define such surfaces, which are not always planar. Long prismatic and equidimensional inclusions frequently occur together in highly varying amounts in such distributions (Fig. 1, VI). The apatite shows a weakly undulating extinction adjacent to these planes/lines. The features described above are observed in apatites in all zones.

Xenotime also occurs as euhedral long prismatic brown crystals, up to one cm long, on the faces of apatites from the core and intermediate zone I. These have their *c* axes parallel or subparallel to the apatite prism face but are otherwise randomly orientated. In intermediate zone I, xenotime is also found as euhedral long prismatic mm-sized brown crystals in calcite "veins" cutting apatite.

In the same zone, colorless euhedral mm-sized xenotimes occur rarely as the latest mineral formed (growing on quartz, muscovite, and rutile) in the replacement of microcline.

Xenotime has been found in only a few samples from intermediate zone III. Two different associations are recognized; xenotime-euxenite-tourmaline-rutile-muscovite and xenotime-euxenite-calcite-muscovite. Muscovitization of the plagioclase is much more pronounced in the latter paragenesis. The xenotime from both parageneses occurs as up to *ca* 2 × 6 mm euhedral crystals with brown color. Microprobe analysis of anhedral inclusions (up to ~ 100 μm across) in the xenotime from the tourmaline association showed Ca, Si, and Ti as the main elements. The inclusions are therefore assumed to be sphene.

The colorless xenotimes have $\omega_{Na} = 1.713 \pm 0.004$ and the yellow xenotimes $\omega_{Na} \gtrsim 1.713 \pm 0.004$.

Monazite

Monazite has been found only as inclusions in apatite. It has been observed in matrix only in

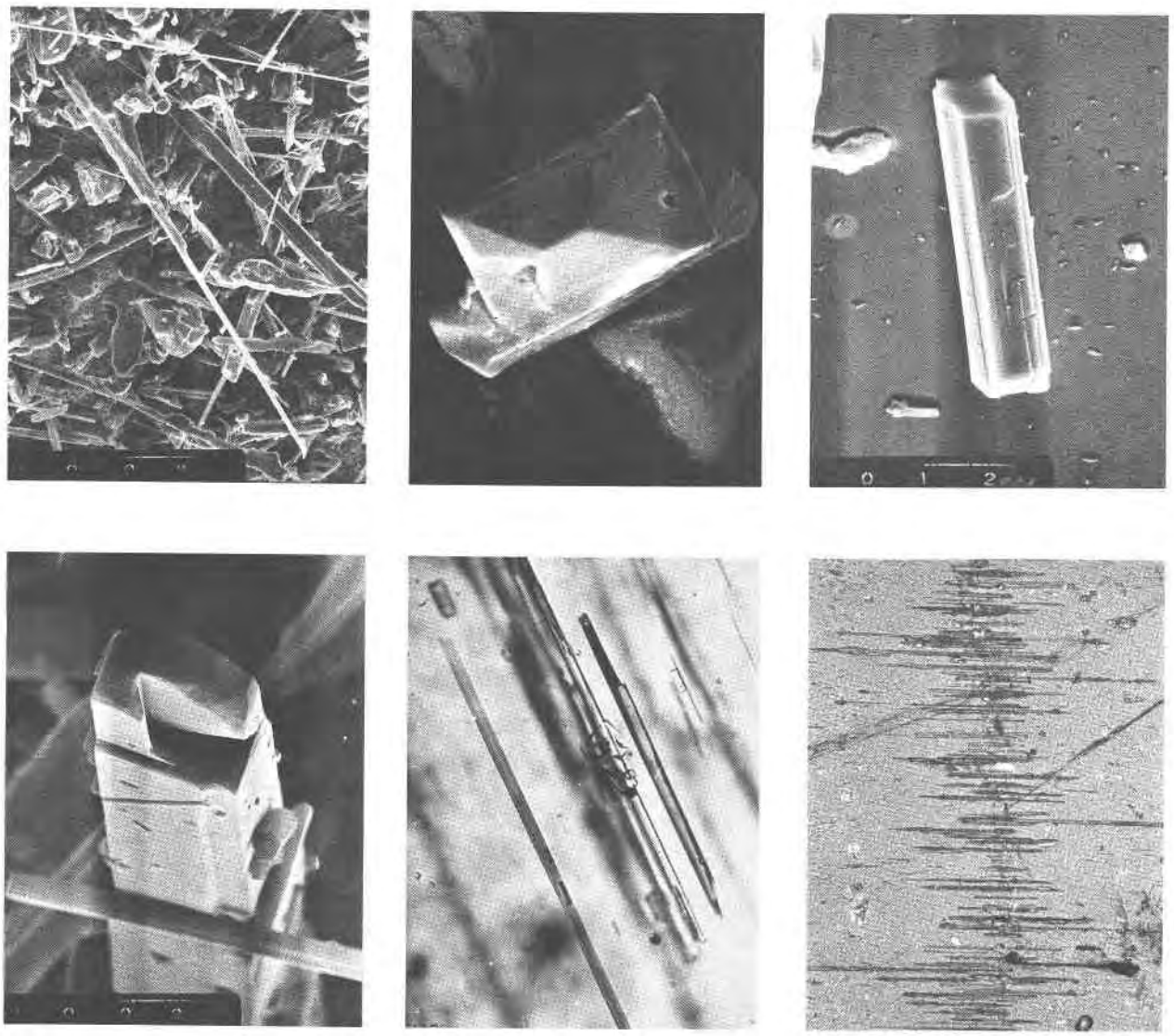

FIG. 1. Inclusions in apatite. I: Scanning electron microscope (SEM) photo (× 400) showing general types of inclusions. II: SEM photo (× 2000) showing a short prismatic xenotime. III and IV: SEM photo (× 3500; × 3000) showing xenotimes with staircase-like terminations. V: Photo (× 500) showing needles of xenotimes oriented parallel to apatite *c* axis. VI: Photo (× 55) showing part of a curved face or line defined by parallel-oriented xenotimes.

material from the quartz core, where it occurs as colorless anhedral grains (up to ~100 μm) in contact with xenotime. It is also present, in amounts <1 percent, in the material dissolved out of the apatite from intermediate zone I. Here it occurs as anhedral yellow grains up to $\frac{1}{2}$ mm across, which are easily distinguished from the xenotimes by their yellow fluorescence under short wave ultraviolet light (not filtered through cobalt-glass). The identification was confirmed by X-ray powder pattern, chemistry, and optics.

Analytical Methods

The analyses have been carried out using an ARL-EMX microprobe with a 52.5° takeoff angle, housed in the Central Institute for Industrial Research, Oslo. The analytical methods and the empirical correction factors used in this study were those described by Åmli and Griffin (1975).

The error bars in the figures (except Fig. 2) correspond to the relative standard deviations quoted by Åmli and Griffin (1975).

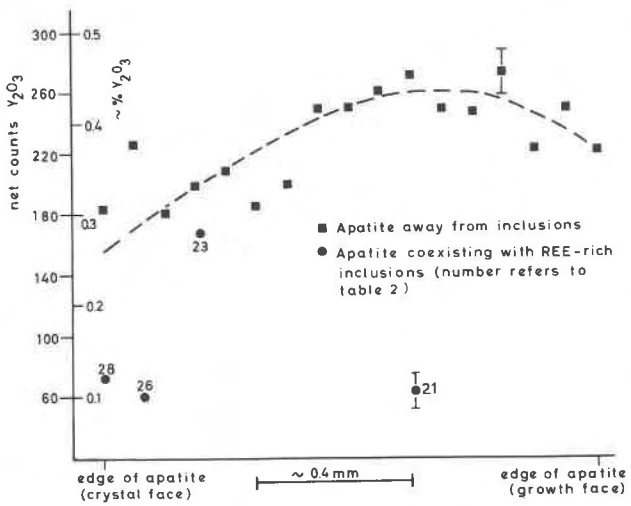

FIG. 2. Yttrium concentration profile ($\perp c$ axis in axial plane) in apatite 69-1 from the quartz core. Note the low Y content for apatite adjacent to rare-earth-rich inclusions. Anomalously high and low Y values in the profile probably arise from interference by xenotime and quartz respectively. A low yttrium content could also be due to the analysis being taken near to a xenotime that has been removed during the cutting. Error bars on a high and low Y value indicate analytical precision. On the "growth face" apatite is in contact with microcline. Simultaneous(?) growth of the two minerals has resulted in an irregular surface probably composed of an oscillatory combination of apatite prism and pyramid forms, as have been seen on large apatite crystals.

Analytical Results

Analyses of xenotimes, monazites, and apatites from the Gloserheia granite pegmatite are presented in Table 2, and Table 3 gives a key to the analyses in Table 2.

In addition to the elements in Table 2, Na, Mg, Fe, Mn, As, Sr, U, and Th have been looked for in several randomly selected samples of each mineral; they are present only in very small amounts (<0.1 wt percent) except for Na, which comprises approximately 0.12 wt percent in apatites having abundant amounts of rare earth inclusions. Ca contents are <0.05 wt percent for xenotimes and monazites included in apatite.

The poor precision for the REE in the apatites analyzed adjacent to REE-rich inclusions precludes detailed discussion of REE distribution for these apatites, since any variations are considered to be within the analytical error. However, Figure 2 shows that the apatite is zoned (asymmetrically?) with respect to yttrium and that the yttrium content is definitely lower for apatite close to the xenotime inclusions, along roughly the same profile. Apatite 85 (anal. no. 8, Table 2), which has almost no REE-rich inclusions, contains 0.71 percent Y_2O_3, compared with a Y_2O_3 content ranging generally between 0.09 and 0.12 wt percent for apatite adjacent to xenotimes. Deviations from this pattern reflect excitation of xenotime inclusions by fluorescence from the continuous spectrum and/or by characteristic fluorescence, as in the case of analyses no. 10 and no. 23 in Table 2.

The lower yttrium content is probably accompanied by a lowering in the content of the rest of the REE, but this is only weakly indicated by the analytical results, because of the poor precision of these analyses.

Zoning is a common feature in all types of xenotimes. Figure 3 shows the zonal variation in Y, Yb, and Gd in a xenotime (68-13, see Tables 2 and 3) included in apatite from intermediate zone III. Y and Yb are enriched in the central parts of the crystal while Gd is depleted. Figure 4 shows the core-normalized REE distribution in the rim and an intermediate position, along the profile shown in Figure 3. As can be seen, there is an increase (if most weight is placed on the elements that have the best analytical precision) in the ratio of the lighter to the heavier REE from the core to the rim in the crystal. Since no data have been obtained for La, Ce, Pr, and Nd, it is not known if these elements show the same relative enrichment in the rim. Cursory studies of other xenotimes (whether included in apatite or not) indicate the presence of the same type of zoning as shown by xen. 68-13. Quite another type of zoning, however, has been found for xen. 29-2m (see Table 3 and Fig. 5). Figure 6 shows that this zoning probably reflects first a decrease in the ratio of light to heavy rare earths and then an increase, so that the REE distribution when crystallization ceased was nearly the same as when it started.

The REE distributions for xenotimes included in an apatite from the quartz core are shown in Figure 7. Because the curves are smoother than the error bars indicate they should be, and because all the analyses were done in the same day, the analytical precision is considered to be much better than is indicated. The ratio of the light to the heavy rare earths in the xenotime inclusions increases from the center of the apatite towards the rim. The only pronounced deviation is the depletion in Nd and Sm in the xenotime located at or very close to the rim of the apatite crystal. The trend seems to be unaffected by the fact that xen. 5 and xen. 3 occur in contact with monazite grains.

Figure 8 shows REE distribution patterns for randomly selected xenotimes included in apatite from

TABLE 2. Electron Microprobe Analysis of Xenotimes, Monazites, and Apatites from Gloserheia Granite Pegmatite

	1		2		3		4		5		6		7	
Element	wt.%	atom. prop.	wt.%	atom. prop.	wt.%	atom. prop.	wt.%	atom. prop.	wt.%	atom. prop.	wt.%	atom. prop.	wt.%	atom. prop.
F	na		na		na		na		3.12	0.8541	na		na	
SiO_2	0.36	0.0123	0.46	0.0154	0.21	0.0071	0.11	0.0039	nd		0.23	0.0077	0.31	0.0104
P_2O_5	34.34	0.9877	34.93	0.9846	34.52	0.9929	34.62	0.9961	40.94	3.0000	35.38	0.9923	34.37	0.9896
CaO	nd		nd		nd		nd		55.11	5.1113	nd		nd	
Y_2O_3	46.35	0.8383	47.21	0.8359	46.25	0.8361	42.48	0.7674	0.09	0.0041	46.13	0.8133	44.03	0.7968
La_2O_3	nd		nd		nd		nd		nd		nd		nd	
Ce_2O_3	nd		nd		nd		nd		0.04	0.0012	nd		nd	
Pr_2O_3	nd		nd		nd		nd		nd		nd		nd	
Nd_2O_3	wv		wv		wv		wv		nd		0.22	0.0026	0.17	0.0020
Sm_2O_3	0.21	0.0024	0.28	0.0032	0.26	0.0030	0.74	0.0087	0.04	0.0012	0.49	0.0056	0.49	0.0057
Eu_2O_3	nd		nd		nd		0.35	0.0041	nd		0.13	0.0015	0.07	0.0008
Gd_2O_3	2.07	0.0234	1.69	0.0187	2.50	0.0282	4.72	0.0532	0.05	0.0015	1.91	0.0211	2.69	0.0303
Tb_2O_3	0.56	0.0063	0.40	0.0044	0.49	0.0054	1.05	0.0117	nd		0.42	0.0046	0.58	0.0064
Dy_2O_3	5.09	0.0557	3.82	0.0410	5.43	0.0594	7.02	0.0768	0.10	0.0027	3.84	0.0410	4.93	0.0540
Ho_2O_3	1.20	0.0130	0.87	0.0092	1.11	0.0119	1.23	0.0133	nd		1.01	0.0107	1.27	0.0137
Er_2O_3	3.67	0.0392	3.60	0.0376	3.43	0.0366	3.47	0.0370	nd		3.78	0.0393	4.05	0.0432
Tm_2O_3	0.59	0.0063	0.62	0.0064	0.67	0.0071	0.61	0.0065	nd		0.68	0.0070	0.70	0.0073
Yb_2O_3	3.77	0.0391	4.04	0.0410	3.18	0.0329	2.93	0.0304	nd		4.25	0.0429	4.36	0.0452
Lu_2O_3	0.55	0.0056	0.59	0.0060	0.41	0.0042	0.38	0.0039	nd		0.86	0.0086	0.87	0.0089
$O \equiv F$									1.31					
Sum	98.74		98.51		98.46		99.71		98.18		99.33		98.89	
Struct. form.	$(REE)_{1.0293}$ $(P,Si)_{1.0000}$		$(REE)_{1.0034}$ $(P,Si)_{1.0000}$		$(REE)_{1.0248}$ $(P,Si)_{1.0000}$		$(REE)_{1.0130}$ $(P,Si)_{1.0000}$		$(Ca,REE)_{5.1220}$ $(P,Si)_{3.0000}$ $F_{0.8541}$		$(REE)_{0.9982}$ $(P,Si)_{1.0000}$		$(REE)_{1.0143}$ $(P,Si)_{1.0000}$	

	8		9		10		11		12		13		14	
Element	wt.%	atom. prop.	wt.%	atom. prop.	wt.%	atom. prop.	wt.%	atom. prop.	wt.%	atom. prop.	wt.%	atom. prop.	wt.%	atom. prop.
F	2.92	0.7931	na		2.96	0.8076	na		na		na		na	
SiO_2	0.49	0.0425	0.41	0.0139	0.60	0.0516	0.44	0.0148	0.17	0.0058	0.26	0.0089	0.28	0.0096
P_2O_5	40.67	2.9575	34.25	0.9861	40.36	2.9484	34.69	0.9852	34.81	0.9942	34.29	0.9911	34.35	0.9904
CaO	54.47	5.0147	nd		54.76	5.0622	nd		nd		nd		nd	
Y_2O_3	0.71	0.0320	46.71	0.8452	0.67	0.0309	45.72	0.8162	46.30	0.8314	47.40	0.8611	47.55	0.8616
La_2O_3	nd		nd		nd		nd		nd		nd		nd	
Ce_2O_3	0.10	0.0035	nd		0.12	0.0036	nd		nd		nd		nd	
Pr_2O_3	nd		nd		nd		nd		nd		nd		nd	
Nd_2O_3	0.12	0.0036	wv		0.18	0.0054	0.09	0.0011	wv		nd		nd	
Sm_2O_3	0.05	0.0014	0.38	0.0044	0.07	0.0021	0.20	0.0023	0.20	0.0023	0.16	0.0019	0.16	0.0019
Eu_2O_3	nd		nd		nd		nd		0.06	0.0007	nd		nd	
Gd_2O_3	0.10	0.0028	2.05	0.0231	0.11	0.0030	1.48	0.0164	1.76	0.0197	1.46	0.0166	1.47	0.0166
Tb_2O_3	nd		0.52	0.0058	0.07	0.0018	0.37	0.0041	0.44	0.0049	0.33	0.0037	0.35	0.0039
Dy_2O_3	0.11	0.0029	4.24	0.0464	0.14	0.0039	3.82	0.0413	4.28	0.0466	3.68	0.0405	3.74	0.0410
Ho_2O_3	nd		0.94	0.0101	nd		0.99	0.0106	1.01	0.0109	0.95	0.0103	1.02	0.0111
Er_2O_3	0.04	0.0010	3.37	0.0360	nd		3.83	0.0404	3.90	0.0414	3.80	0.0408	3.78	0.0405
Tm_2O_3	nd		0.47	0.0049	nd		0.67	0.0070	0.66	0.0069	0.61	0.0065	0.63	0.0066
Yb_2O_3	0.08	0.0020	4.24	0.0439	0.09	0.0024	4.66	0.0477	4.56	0.0469	4.46	0.0464	4.44	0.0461
Lu_2O_3	nd		0.81	0.0083	nd		0.95	0.0097	0.61	0.0062	0.59	0.0061	0.62	0.0064
$O \equiv F$	1.23				1.24									
Sum	98.63		98.44		98.89		97.91		98.76		97.99		98.39	
Struct. form.	$(Ca,REE)_{5.0639}$ $(P,Si)_{3.0000}$ $F_{0.7931}$		$(REE)_{1.0281}$ $(P,Si)_{1.0000}$		$(Ca,REE)_{5.1153}$ $(P,Si)_{3.0000}$ $F_{0.8076}$		$(REE)_{0.9968}$ $(P,Si)_{1.0000}$		$(REE)_{1.0174}$ $(P,Si)_{1.0000}$		$(REE)_{1.0339}$ $(P,Si)_{1.0000}$		$(REE)_{1.0357}$ $(P,Si)_{1.0000}$	

different zones in the pegmatite. Also shown is the REE distribution for a xenotime partly embedded in the prism face of an apatite from intermediate zone I. This pattern of increasing relative enrichment in the lighter REE from the outer zone of the pegmatite towards the core is analogous to that observed from the center to the rim of a single apatite crystal and shown in Figure 7. Xenotime 84 also fits this scheme, as can be more easily seen from Figure 9. From Figures 7 and 8 it is furthermore seen that the degree

TABLE 2, Continued

	15		16		17		18		19		20		21	
Element	wt.%	atom. prop.	wt.%	atom. prop.	wt.%	atom. prop.	wt.%	atom. prop.	wt.%	atom. prop.	wt.%	atom. prop.	wt.%	atom. prop.
F	na		na		na		na		na		na		3.89	1.0377
SiO_2	0.32	0.0109	0.34	0.0117	0.22	0.0076	0.28	0.0096	0.18	0.0063	0.68	0.0272	na	
P_2O_5	34.19	0.9891	34.25	0.9883	34.35	0.9924	34.28	0.9904	34.49	0.9937	28.66	0.9728	42.01	3.0000
CaO	nd		nd		nd		nd		nd		nd		55.52	5.0175
Y_2O_3	47.88	0.8706	47.71	0.8654	47.13	0.8512	46.46	0.8438	43.78	0.7925	0.96	0.0204	0.10	0.0048
La_2O_3	nd		nd		nd		nd		nd		11.05	0.1633	nd	
Ce_2O_3	nd		nd		nd		nd		nd		32.19	0.4725	nd	
Pr_2O_3	nd		nd		nd		nd		nd		5.71	0.0834	nd	
Nd_2O_3	nd		nd		nd		nd		0.32	0.0039	17.73	0.2538	0.06	0.0018
Sm_2O_3	0.11	0.0013	0.20	0.0024	0.23	0.0027	0.23	0.0027	0.61	0.0071	2.61	0.0360	nd	
Eu_2O_3	nd		nd		nd		nd		0.11	0.0013	nd		nd	
Gd_2O_3	1.23	0.0139	1.39	0.0157	1.63	0.0183	1.77	0.0200	2.69	0.0304	0.75	0.0099	0.06	0.0018
Tb_2O_3	0.25	0.0028	0.34	0.0038	0.42	0.0047	0.42	0.0047	0.57	0.0063	nd		nd	
Dy_2O_3	3.60	0.0397	3.58	0.0393	3.91	0.0427	4.19	0.0461	4.80	0.0526	0.27	0.0034	nd	
Ho_2O_3	0.84	0.0091	1.05	0.0114	1.02	0.0111	1.00	0.0108	1.24	0.0134	0.16	0.0020	nd	
Er_2O_3	3.64	0.0391	3.88	0.0415	3.61	0.0385	3.86	0.0414	4.17	0.0446	0.07	0.0008	nd	
Tm_2O_3	0.58	0.0061	0.65	0.0069	0.60	0.0064	0.68	0.0072	0.71	0.0075	nd		nd	
Yb_2O_3	4.41	0.0459	4.48	0.0466	4.26	0.0441	4.49	0.0467	4.70	0.0487	0.10	0.0012	0.06	0.0015
Lu_2O_3	0.58	0.0060	0.66	0.0068	0.55	0.0056	0.60	0.0062	0.90	0.0092	nd		nd	
$O \equiv F$													1.63	
Sum	97.63		98.53		98.12		98.26		99.27		100.94		100.07	
Struct. form.	$(REE)_{1.0345}(P,Si)_{1.0000}$		$(REE)_{1.0398}(P,Si)_{1.0000}$		$(REE)_{1.0253}(P,Si)_{1.0000}$		$(REE)_{1.0296}(P,Si)_{1.0000}$		$(REE)_{1.0175}(P,Si)_{1.0000}$		$(REE)_{1.0467}(P,Si)_{1.0000}$		$(Ca,REE)_{5.0274}(P,Si)_{3.0000}F_{1.0377}$	

	22		23		24		25		26		27		28	
Element	wt.%	atom. prop.	wt.%	atom. prop.	wt.%	atom. prop.	wt.%	atom. prop.	wt.%	atom. prop.	wt.%	atom. prop.	wt.%	atom. prop.
F	na		3.80	1.0190	na		na		3.85	1.0297	na		4.11	1.1067
SiO_2	0.25	0.0087	na		0.22	0.0075	0.51	0.0206	na		0.17	0.0057	na	
P_2O_5	33.68	0.9913	41.79	3.0000	34.38	0.9925	28.53	0.9794	41.90	3.0000	34.88	0.9943	41.62	3.0000
CaO	nd		55.39	5.0325	nd		nd		55.65	5.0436			55.64	5.0760
Y_2O_3	43.12	0.7977	0.28	0.0129	43.47	0.7877	0.87	0.0187	0.10	0.0048	43.96	0.7875	0.12	0.0051
La_2O_3	nd		nd		nd		9.38	0.1402	nd		nd		nd	
Ce_2O_3	nd		nd		nd		30.77	0.4567	nd		nd		nd	
Pr_2O_3	nd		nd		nd		5.82	0.0859	nd		nd		nd	
Nd_2O_3	0.35	0.0044	0.10	0.0030	0.48	0.0059	20.83	0.3016	0.06	0.0018	0.21	0.0026	0.08	0.0024
Sm_2O_3	0.61	0.0073	nd		0.87	0.0102	3.59	0.0501	nd		0.73	0.0085	nd	
Eu_2O_3	0.09	0.0010	nd		0.12	0.0014	nd		nd		0.24	0.0027	nd	
Gd_2O_3	2.67	0.0308	0.05	0.0015	2.86	0.0323	0.83	0.0111	0.05	0.0015	3.59	0.0402	0.07	0.0018
Tb_2O_3	0.55	0.0062	nd		0.55	0.0062	nd		nd		0.70	0.0078	nd	
Dy_2O_3	4.77	0.0534	nd		4.66	0.0511	0.20	0.0026	nd		5.41	0.0587	nd	
Ho_2O_3	1.23	0.0135	nd		1.18	0.0128	nd		nd		1.25	0.0133	nd	
Er_2O_3	3.99	0.0436	nd		3.88	0.0415	nd		nd		3.83	0.0405	nd	
Tm_2O_3	0.75	0.0081	nd		0.65	0.0069	nd		nd		0.65	0.0068	nd	
Yb_2O_3	4.65	0.0493	0.09	0.0021	4.31	0.0448	0.09	0.0011	nd		3.73	0.0383	0.07	0.0018
Lu_2O_3	0.85	0.0089	nd		0.82	0.0084	nd		nd		0.62	0.0063	nd	
$O \equiv F$			1.60						1.62				1.73	
Sum	97.56		99.90		98.45		101.42		99.99		99.97		99.98	
Struct. form.	$(REE)_{1.0242}(P,Si)_{1.0000}$		$(Ca,REE)_{5.0520}(P,Si)_{3.0000}F_{1.0190}$		$(REE)_{1.0092}(P,Si)_{1.0000}$		$(REE)_{1.0680}(P,Si)_{1.0000}$		$(Ca,REE)_{5.0517}(P,Si)_{1.0000}F_{1.0297}$		$(REE)_{1.0132}(P,Si)_{1.0000}$		$(Ca,REE)_{5.0871}(P,Si)_{1.0000}F_{1.1067}$	

Atom. prop. are normalized to P + Si = 1 for xenotimes and monazites and P + Si = 3 for apatites.
wv: Wild value. nd: Not detected. na: Not analyzed.

TABLE 3. Key to Analyses in Table 2

Anal. no.	Sample	Mineral, paragenesis etc.	Remarks
1	81-m	Euhedral xenotime (mm-sized), associated with tourmaline, rutile, euxenite and muscovite in int. zone III. Sphene is found as inclusions.	Analysis represents average of 10-15 spots (because of an irregular inhomogenity) for each element on a cross section near the center of the crystal.
2-4	68-13, xen. 1-3	Core, intermediate and rim respectively of a subhedral xenotime (~50x80μ), included in an anhedral apatite from int. zone III.	Oriented with the c-axis parallel to the apatite c-axis. Shows positive elongation.
5	68-13, ap.	Apatite adjacent to xen. 68-13.	Counts from several spots in a region ~15μ from the xenotime inclusion.
6	P3/68-12	Euhedral xenotime (½x1mm) associated with muscovite euxenite and calcite in int. zone III.	Analyses are from an area of approx. 5x5μ, assumed to be from near the center of the crystal.
7	84	Euhedral xenotime (mm-sized) from the prism face of an apatite from int. zone I.	Average of 8 analyses (Åmli & Griffin, 1975). Each analysis are from the same area of approx. 30x30μ, carefully chegued for homogenity.
8	85	Euhedral dark green apatite from int. zone I.	Arithmetic mean of three analyses of grains taken out of approx. 1/4 cm^3 apatite. The apatite has very few inclusions.
9	69-S2 m, xen. 4	Euhedral xenotime included in apatite from int. zone I.	Oriented with c-axis parallel to the apatite c-axis. 4.27% apatite is subtracted from analysis.
10	69-S2 m, ap. 4	Apatite adjacent to 69-S2 m, xen. 4.	Counts from several spots ~15μ from the crystal.
11	P5/69-13-1	Euhedral xenotime (mm-sized) from a fracture in apatite with newly formed apatite, plus calcite and hematite. Int. zone I.	The analysis is assumed to be from near the center of the crystal and are from an area of approx. 5x5μ.
12-18	Q1/29-2 m no. 1-7	Euhedral xenotime (mm-sized) associated with quartz, muscovite and rutile in altered parts of int. zone I microcline.	The analyses are from a cross section (~1/4x1/2 mm) near the center of the crystal. No. 1 is at the center and no. 7 at the rim of the crystal. The distance between the analysed points are roughly equal.
19	69-1, xen. 5	Subhedral xenotime (~100x200μ) included in a euhedral apatite (1.4x1.8 cm) from the quartz core. (All the following are from the same apatite).	Elongation is perpendicular to the apatite c-axis. Direction of the xenotime c-axis has not been determined because of interference from underlying monazite. The xenotime is located in the center of the apatite and approx. 8000μ from the prism face. Analysis is from the center of the xenotime. 0.16% ap. is subtracted from the analysis.

of enrichment in light rare earths from intermediate zone III to the core of the pegmatite is much greater than from the core to the rim of the apatite crystal from the quartz core.

Considering the REE distribution patterns obtained for the xenotimes not included in apatite (see Fig. 9), it is obvious that the regular fractionation trend seen in the xenotimes included in apatite is absent. Other deviations are the decrease in the absolute amount of the lighter REE and the lower ratio of light to heavy REE for these xenotimes (except 68-12) relative to those included in apatite from the same zones.

Discussion

This discussion will consider (a) origin of inclusions of rare earth minerals in apatite, (b) rare earth fractionation in the apatite-xenotime-monazite system, and (c) rare earth fractionation for xenotimes not included in apatite.

TABLE 3, Continued

Anal. no.	Sample	Mineral, paragenesis etc.	Remarks
20	69-1, mon. 5	Anhedral monazite (~100x300μ) in contact with 69-1, xen. 5.	Analysis is from approx. the same spot. 1.38% apatite has been subtracted from the analysis.
21	69-1, ap. 5	Apatite adjacent to 69-1 xen./mon. 5.	Counting on several spots approx. 15μ from the xen./mon. inclusion.
22	69-1, xen. 4	Subhedral xenotime (~20x200μ).	Oriented with c-axis parallel to the apatite c-axis. Distance from apatite prism face is 2500μ. 0.61% apatite is subtracted from the analysis.
23	69-1, ap. 4	Apatite adjacent to 69-1, xen. 4.	Counting on several spots approx. 15μ from the xen. inclusion.
24	69-1, xen. 3	Anhedral xenotime (~20x30μ).	Oriented with c-axis parallel to the apatite c-axis. Distance from apatite prism face is 1000μ. 0.49% apatite is subtracted from the analysis.
25	69-1, mon. 3	Anhedral monazite (~10x30μ) in contact with 69-1, xen. 3.	Analysis is from approx. the same spot. 1.98% apatite subtracted from the analysis.
26	69-1, ap. 3	Apatite adjacent to 69-1, xen./mon. 3.	Counting on several spots approx. 15μ from the xen./mon. inclusion.
27	69-1, xen. 2	Anhedral xenotime (~30x80μ).	C-axis is not parallel to apatite c-axis. Located very close to the apatite prism face, probably less than 50μ (the uncertainty is related to removal of apatite during cutting and polishing). Analysis is from center of the grain in an area of approx. 5x5μ. 0.14% apatite subtracted from analysis.
28	69-1, ap. 2	Apatite adjacent to 69-1, xen. 2.	Counted at several spots approx. 15μ from the xen.

Origin of Inclusions of Rare Earth Minerals in Apatite

A simplified approach to the problem of formation of inclusions of rare earth minerals in apatite is given by the following models:

I. The rare earth minerals formed before the apatite that locally surrounds them, and were deposited on the growing faces.
II. The rare earth minerals crystallized simultaneously and in contact with the growing apatite.
III. The rare earth minerals formed after the apatite by a. exsolution, or b. exsolution + metasomatism.

These three models have been considered partly because inclusions in minerals (with a mutual orientation of the two crystal structures) can originate from growth of the "included crystals" on the faces of the host mineral; various examples are summarized by Seifert (1953). Staircase-like crystal morphology due to simultaneous growth of two minerals (in contact) has been described by Haynes (1959), and the forms observed on some of the xenotimes (III and IV, Fig. 1) could have originated in such a way. On the other hand, oriented "inclusions" in minerals are often considered to be exsolution phenomena; for instance vein perthites (Laves and Soldatos, 1963) and orthopyroxene lamellae in clinopyroxene (Bown and Gay, 1960),

If the xenotimes, in accordance with model I, formed separately from the apatite, the low content of rare earths in apatite adjacent to xenotime inclusions (see Fig. 2) cannot be explained. If, however, the xenotimes formed very close to the growing apatite, and very rapidly, this could deplete the mineral-forming fluid in REE, and lower the REE content of the apatite. According to Jahns (1953) and Schneiderhöhn (1961), giant crystals (such as some of

the apatites) are believed to have formed in a volatile-rich silicate melt of very low viscosity, with rapid diffusion of components and formation of few crystal nuclei. If this is true, it *seems* likely that the liquid would reequilibrate (at least on the scale in discussion) faster than the apatite could grow and hence the apatite would show no depletion in the rare earths around the xenotimes. Furthermore, Jahns' (1953) and Schneiderhöhn's (1961) proposal that very few nuclei were formed has definitely not been the case for the xenotimes. For these reasons it is assumed that model I cannot explain the formation of the rare earth minerals included in apatite.

Model II is rejected for the obvious reason that the apatite on one side of the xenotime must have crystallized before the inclusion, and hence is not likely to be depleted in REE (as shown by Fig. 2) even if the apatite crystallizing simultaneously with the xenotime was depleted.

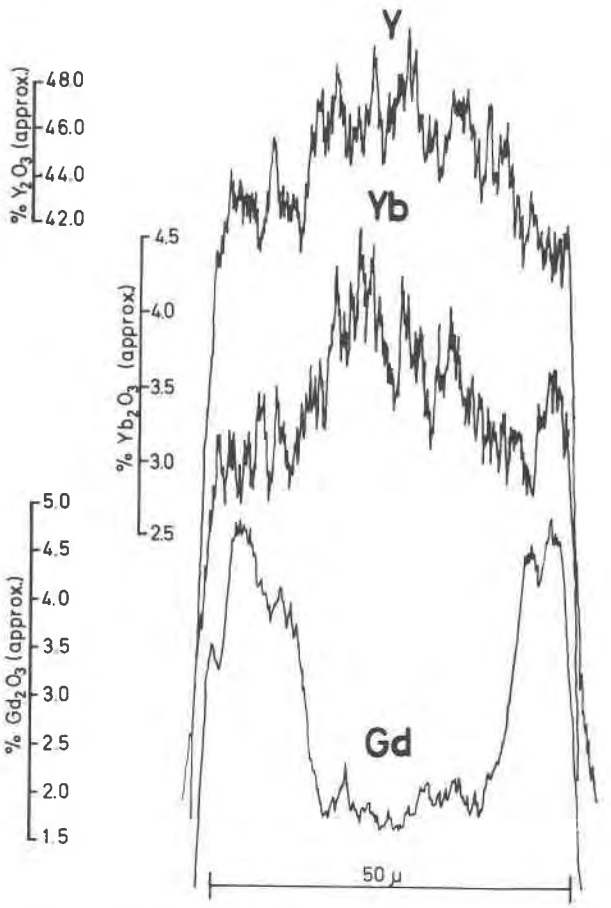

FIG. 3. Electron microprobe scans showing Y, Yb, and Gd distribution in a profile $\perp c$ axis for 68-13/xenotime 1 included in apatite from intermediate zone III. The more irregular curves for Y and Yb are due to increased recorder sensitivity.

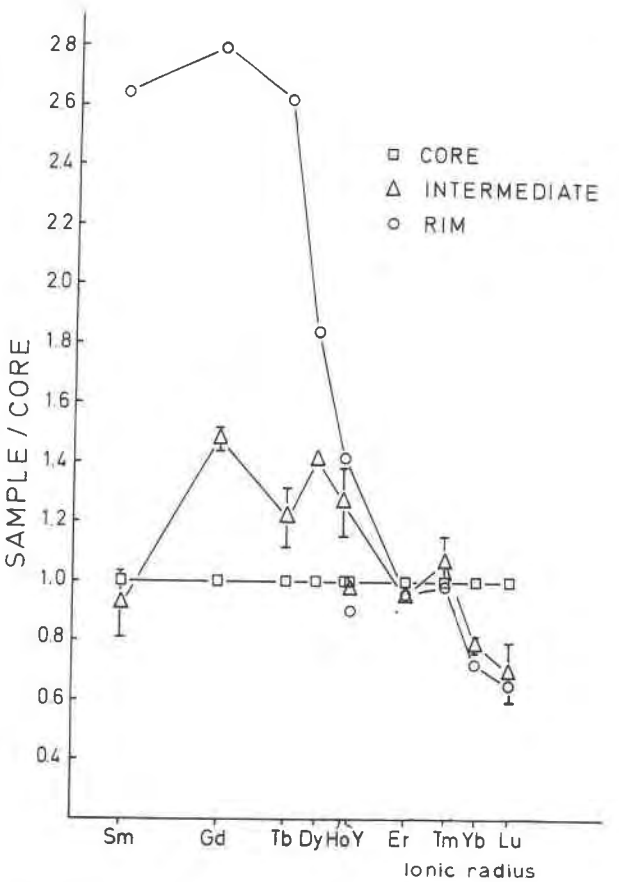

FIG. 4. Spot analyses in the core, intermediate region, and rim of 68-13/xenotime 1 (along the same profile as shown in Fig. 3) normalized to the core composition. In this and the following comparison diagrams, ionic radii are for REE^{3+} in 8-coordination (Shannon and Prewitt, 1969).

If we now consider model IIIa, it is quite clear that rare earth minerals starting to exsolve from the apatite could deplete the surrounding apatite in REE. Exsolution could take place as temperature fell, and be due to oversaturation of the apatite with rare earths. However, several authors (Rass, 1964; Lindberg and Ingram, 1964; Young *et al,* 1969; Young and Munson, 1966; Lyakovich, 1962; Denisov *et al,* 1961; and Omori and Konno, 1962) report apatites that have total REE contents similar to, or higher than, those in the Gloserheia apatites and yet contain no rare earth mineral inclusions. Of these apatites, only that described by Omori and Konno is enriched in the heavy REE; the others are enriched in the light REE. In view of the REE distribution of the apatite described by Omori and Konno, and the presence of monazite inclusions in the Gloserheia pegmatite, it is assumed that any exsolution is not

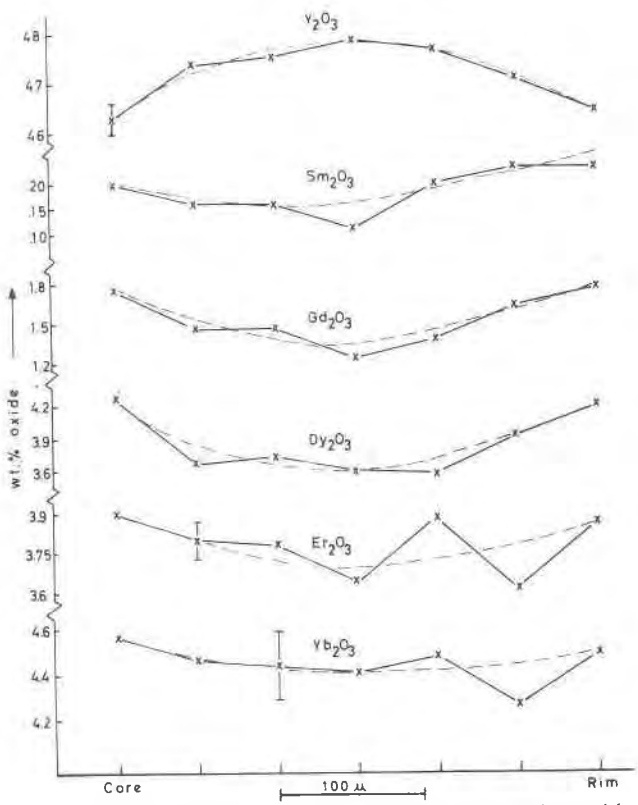

FIG. 5. Variation for some selected rare earth oxides (those with best analytical precision) from the core to rim in a cross section (~¼ × ½ mm) near the center of a xenotime (29-2m, see Table 3) associated with muscovite, quartz, and rutile in replacements of microcline in intermediate zone I. Error bars for Sm, Gd, and Dy equal the size of the cross.

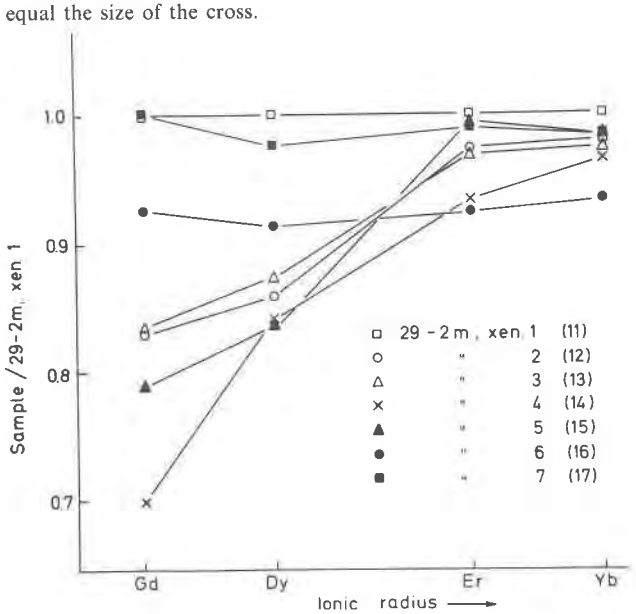

FIG. 6. REE distribution patterns (for some selected rare earth oxides) in a cross section (~¼ × ½ mm) near the center of a xenotime (29-2m, see Table 3) associated with muscovite, quartz, and rutile in replacements of microcline in intermediate zone I. Numbers in parentheses refer to Table 2.

controlled primarily by the distribution of the rare earths. The apatites with no rare earth mineral inclusions may have cooled under conditions which did not promote exsolution.

For an exsolution model several mechanisms, each involving non-stoichiometry, can be considered.

According to Cruft, Ingamells, and Muysson (1965), apatite has the following structural positions: A(Ca,REE. . . . .), B(P,Si . . . .), C(O), D(F,Cl . . . .) with the stoichiometric proportions: $A_5B_3C_{12}D_1$. If xenotime or monazite exsolve from a stoichiometric apatite, elements in the A, B, and C positions are removed in the atomic proportions 1:1:4. The result will be an apatite with vacant sites in the A, B, and C positions. Exsolution of the other phases identified in the apatite would enhance this non-stoichiometry.

The following schematic reactions can thus be set

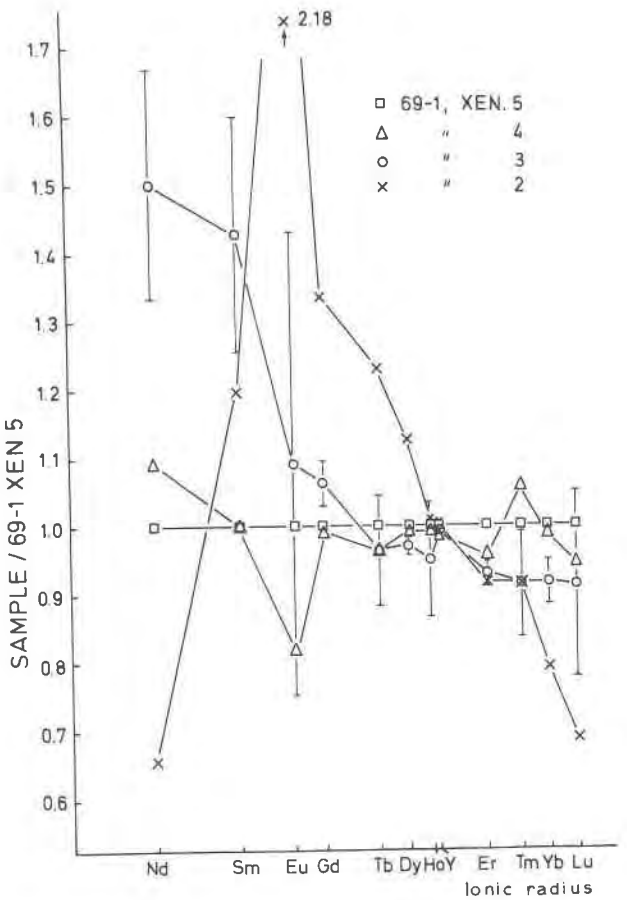

FIG. 7. REE distribution patterns of xenotimes included in an apatite crystal (69-1) from the quartz core. Xenotime 5 is located approximately in the center of the crystal, xenotime 2 at the rim or very close to the rim, and the others in intermediate positions (see Table 3 for further details). The analyses are normalized to the composition of the xenotime in the core of the apatite.

up for the exsolution of xenotime/monazite from apatite:

$$\langle 1\rangle \quad \underset{\text{stoichiometric apatite}}{A_5B_3C_{12}D_1} \rightarrow \underset{\text{non-stoichiometric apatite}}{A_{5-x}B_{3-x}C_{12-4x}D_1} + \underset{\text{xenotime-monazite}}{A_xB_xD_{4x}}$$

$$\langle 2\rangle \quad \underset{\text{non-stoichiometric apatite}}{A_{5+x}B_{3+x}C_{12+4x}D_1} \rightarrow \underset{\text{stoichiometric apatite}}{A_5B_3C_{12}D_1} + \underset{\text{xenotime-monazite}}{A_xB_xD_{4x}}$$

$$\langle 3\rangle \quad \underset{\text{non-stoichiometric apatite}}{A_5B_{3+x}C_{12+4x}D_1} \rightarrow \underset{\text{non-stoichiometric apatite}}{A_{5+\frac{x}{2}}B_{3+\frac{x}{2}}C_{12+2x}D_1} + \underset{\text{xenotime-monazite}}{A_xB_xD_{4x}}$$

The principles would be the same if exsolution of quartz and plagioclase is taken into account. Obviously one could complicate the picture by postulating non-stoichiometry in the exsolved phases as well, but adjustment of a high-temperature non-stoichiometry in the apatite by exsolution at lower temperature seems to offer a satisfactory explanation of the inclusions. Unfortunately the precision of the analytical data does not allow distinction among possibilities ⟨1⟩–⟨3⟩.

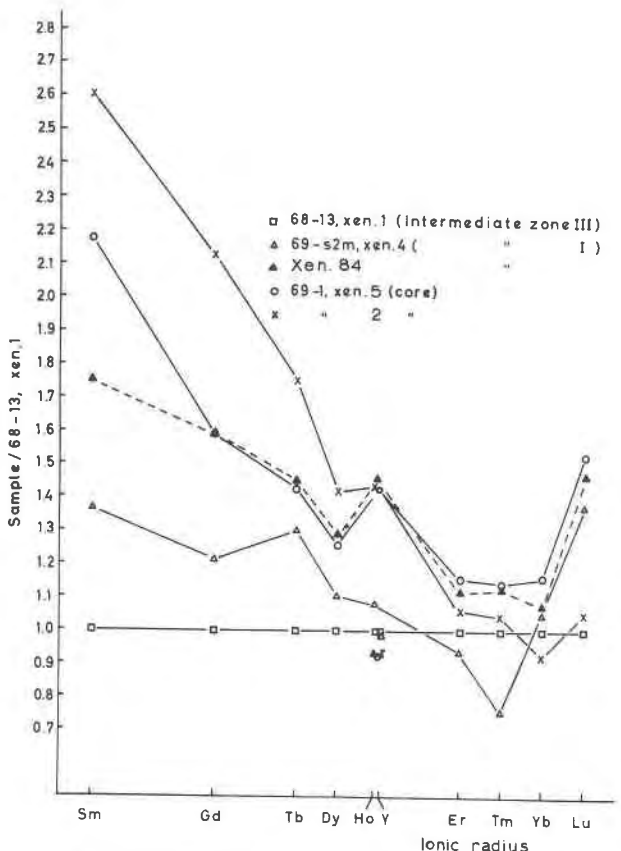

FIG. 8. REE distribution patterns for xenotimes included in apatites from intermediate zones III, I, and from the core, normalized to the intermediate zone III xenotime. REE distribution patterns for xenotime 84 (not included in apatite) are shown for comparative purposes.

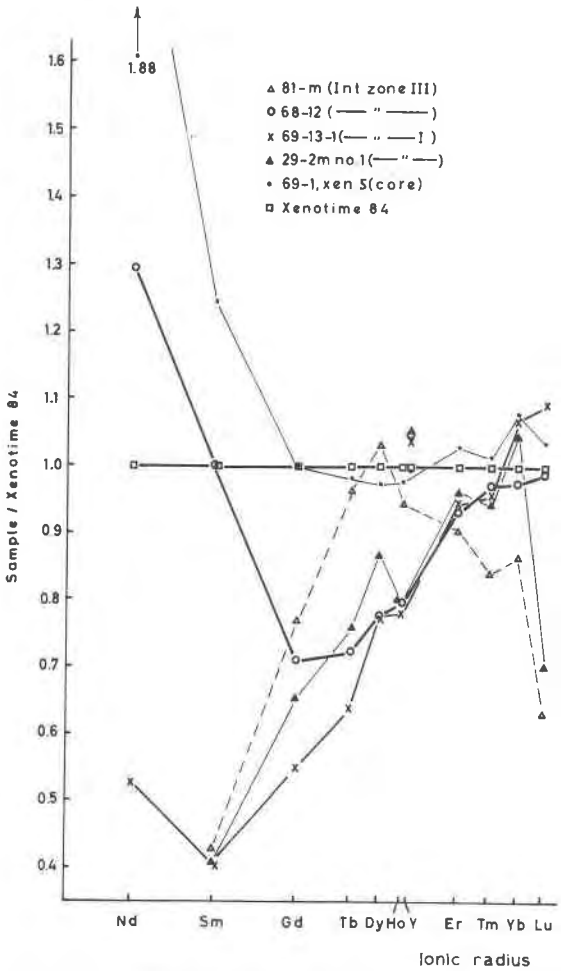

FIG. 9. REE distributions for xenotimes not included in apatite. For comparative purposes the REE distribution for xenotime 5 (included in apatite 69-1 from the quartz core) is also shown. See Table 3 for further details on the occurrence of the different xenotimes. Lines connect the rare earth values (excluding Y) for each xenotime.

Exsolution is assumed to take place preferentially at crystal defects (Rast, 1965). Irregular distribution of such defects could then explain the spatial distribution of the inclusions.

A xenotime exsolving from the apatite would prefer the heavy, rather than the light, REE. The surrounding apatite would be steadily enriched in the light relative to the heavy REE, so that during its growth the xenotime would have access to a continuously increasing ratio of light to heavy REE. Model IIIa is therefore in accordance with the zoning actually observed in the xenotimes (see Fig. 3).

The most probable explanation for formation of the monazites is that monazite started to grow after the adjacent xenotime was formed. This is supported by the fact that, after the xenotime was formed as

mentioned above, the apatite would be enriched in the light rare earths, which are preferentially taken up by monazite. Another fact supporting this explanation is the occurrence of monazite only in contact with xenotime.

Model IIIb implies that the REE in the xenotime/monazite have been supplied by a combination of (1) extraction from the apatite and (2) supply by solutions in microfissures in the apatite. It thus conforms to the observed depletion in rare earths in apatite adjacent to xenotime/monazite.

The "advantage" of postulating a metasomatic process in addition to the exsolution process is that the phases present before and after exsolution could be completely stoichiometric, because transport of material in and out of the "apatite-included minerals" system is allowed. A metasomatic process might also explain why previously reported apatites that have total contents of rare earths similar to, or higher than, those in the Gloserheia apatites do not contain inclusions of rare earth minerals.

The zoning in the xenotimes cannot be explained by the metasomatic process alone, whether this is of a diffusion or an infiltration type, in the terms used by Korzhinskij (1965). According to Korzinskij's model, the solid solution series would remain close to constant in composition in each metasomatic zone during infiltration metasomatism. It also seems unlikely that a diffusion metasomatism, allowing compositional variations for solid solution series, could produce the large variations in REE fractionation from the core to rim in a single xenotime crystal while also producing the smaller variations found between xenotimes at the core and rim of a single apatite crystal (see Figs. 4 and 7). The *zoning* in the xenotimes, at least, is therefore considered to be caused by a mechanism such as that proposed under model IIIa.

Some of the inclusions are found crossing minor cracks in the apatite (Fig. 1, VI), thus supporting model IIIb. However, many of the xenotimes are found isolated in the apatite. If material transport along fissures was important for the formation of these xenotimes, the fissures must have healed at some later time.

The data are insufficient to decide whether the inclusions have formed in accordance with model IIIa or IIIb. The following discussion considers model IIIa and shows it to be consonant with several explanations for the REE fractionation found for xenotimes included in apatite from different zones in the pegmatite. An attempt to explain the fractionation in accordance with model IIIb is considered to be too speculative since even more variables are uncontrolled.

Rare Earth Fractionation in the Apatite-Xenotime-Monazite System

In the previous section the zoning in the xenotimes was explained in light of an exsolution model for their formation. The next question that arises is what process or processes have caused the increase in the ratio of light to heavy rare earths in the xenotimes (analyses considered to be from the central part of the crystals), when comparing xenotimes included in apatite from intermediate zone III–intermediate zone I–quartz core (at center of apatite)–quartz core (at rim of apatite) (see Figs. 7 and 8).

It is assumed that the apatites formed successively from the outer towards the inner zone, and that apatite formation was completed in each zone before it began in the next inner zone (*cf* Fersman, 1952, Cameron *et al,* 1949; Schneiderhöhn, 1961; and Jahns and Burnham, 1969).

If the pegmatite was an open system at least during the formation of the apatites, the REE fractionation could be explained by a continuous increase in the ratio of light to heavy REE available to the apatites during their formation. As crystallization proceeded, the apatites would incorporate increasingly lighter REE, a trend which then would be reflected in the xenotimes which exsolved afterwards.

According to Mineyev (1963), however, the same fractionation can be obtained even if the REE distribution was constant during the formation of the apatites. Mineyev suggests from theoretical, experimental, and geological evidence that REE fractionation can be caused by changes in the pH of a solution that carries the REE as complexes, with F^-, Cl^-, CO_3^{2-}, PO_4^{3-}, *etc* as possible ligands. Changes in the pH of this solution may cause a selective breakdown of the REE complexes and hence a selective incorporation into the solid phases.

According to this model the REE fractionation observed in the xenotimes from Gloserheia implies that the pH of the fluid phase increased as crystallization of the apatites proceeded. This would agree with the interpretation of Yermakov (1964) that a stage with an increase in the pH of the solutions appears below the α-β quartz transformation temperature. The mechanism proposed by Mineyev (1963) for REE fractionation is also partly supported by Khomyakov (1967), who, however, favors only a "weak" pH control on this fractionation. Schilling and Winchester (1967) also point out the possibility

that REE fractionation during late stage differentiation (pegmatites) is controlled by REE complexing in a volatile-rich environment.

The takeup of REE by other quantitatively important minerals in the pegmatite (euxenite and allanite in intermediate zone III, and allanite in intermediate zone I) would be an additional complication, if these crystallized simultaneously with the apatites. Because of the regular trend and rather small absolute variations in the observed REE distributions, and since euxenite and allanite, judging from rough estimates, must contain the bulk of the total REE in the pegmatite, it is reasonable to infer that these minerals did not crystallize during the same period as the apatites.

The REE fractionation can also be explained if the pegmatite was a closed system during the formation of the apatites. Apatite, forming successively from the outer towards the inner zone, may have preferentially incorporated heavy REE and thereby enriched the mineral-forming fluid in the light REE. The xenotimes exsolving from these apatites would inherit this fractionation trend (Figs. 7, 8), provided the partition coefficient for REE between apatite and xenotime was more or less constant during exsolution. The mechanism of Mineyev (1963) would be in accordance with this explanation, provided there was an increase in the pH as crystallization of the apatites proceeded.

The fit of the REE distribution for xenotime 84 (not included in apatite) to the trend for the xenotimes included in apatite may indicate that any differences for rare earth partition between (a) liquid-apatite and apatite-xenotime and (b) liquid-xenotime more or less balance out.

Rare Earth Fractionation of Xenotimes not Included in Apatites

The trend in rare earth fractionation shown by xenotimes included in apatite is not observed in the other xenotimes (Fig. 9).

Assuming the pegmatite to be a closed system (during the formation of these xenotimes), the absence of this trend could show that the xenotimes formed at a later stage or stages (the pneumatolytic-hydrothermal stages of Schneiderhöhn, 1961, and others) than the apatites. This may have been during or partly during the same period when euxenite (and allanite in intermediate zone III?) was formed and later altered, with accompanying variations in the REE distribution in the residual fluid. Late formation of these xenotimes is also indicated by their mode of occurrence and their characteristic association with muscovite, rutile, and calcite. Schneiderhöhn (1961) considers euxenite to form during a pneumatolytic stage, and to be altered during a hydrothermal stage with release of Ti. This titanium could have been the source of the rutile found in the pegmatite, very often associated with the xenotimes in question.

The possibility of a pH-control on the REE takeup by the xenotimes (Mineyev, 1963) could also be considered. Changes in pH might be caused by crystallization of OH-bearing phases, such as muscovite and biotite, in the local environment around the different xenotimes. This could happen whether the pegmatite was an open or a closed system during formation of the xenotimes. This hypothesis is supported to some extent by the observed changes in REE-fractionation in the xenotimes that formed together with muscovite and quartz during replacement of microcline (Figs. 5 and 6).

Other studies on REE fractionation in similar mineral systems are unsatisfactory for a comparison with this work. In general, too little is specified about the mineral parageneses, the homogeneity of the analyzed minerals, the location of the analyzed material within the crystals, and other important factors.

Any conclusions on mechanisms and causes for the rare earth fractionations observed must be speculative. However, it seems probable that fractionation in the apatite-xenotime-monazite system, as defined by the observed fractionation for the xenotime inclusions, was caused by processes related only to the continuous crystallization of the apatite-bearing zones towards the center of the pegmatite. This is in accordance with the proposed sequences of crystallization for similar mineral assemblages in other zoned granitic pegmatites (Jahns, 1953; Schneiderhöhn, 1961, *etc*). In contrast, the rare earth fractionation in the other xenotimes probably has a more complex relation to the sequence of the zones in the pegmatite.

In light of the data obtained in this work, it seems clear that careful analytical work in microscopic domains can contribute significantly to our understanding of pegmatite genesis.

Acknowledgments

I wish to express my sincere thanks to Dr. W. L. Griffin, Professor H. Neumann, and B. B. Jensen for stimulating discussions and advice during this work. The electron microprobe analyses were supported by Norges Teknisk Naturvitenskapelige Forskningsråd (NTNF), and scanning electron microscope facilities were generously made available by JEOL-Scandinavia.

References

ALBEE, A. L., AND L. RAY (1970) Correction factors for electron probe microanalysis of silicates, oxides, carbonates, phosphates, and sulfates. *Anal. Chem.* **42,** 1408–1414.

ÅMLI, R., AND W. L. GRIFFIN (1975) Microprobe analysis of REE minerals using empirical correction factors. *Am. Mineral.* **60,** 599–606.

ANDERSEN, O. (1926) Feltspat I. *Norges Geol. Undersøkelse,* **128a,** 142 p.

——— (1931) Feltspat II. *Norges Geol. Undersøkelse,* **128b,** 1–109.

BENCE, A. E., AND A. L. ALBEE (1968) Empirical correction factors for the electron microanalysis of silicates and oxides. *J. Geol.* **76,** 382–403.

BOWN, M. G., AND P. GAY (1960) An X-ray study of exsolution phenomena in the Skaergaard pyroxenes. *Mineral. Mag.* **32,** 379–388.

BROCH, O. A. (1963) Age determinations of Norwegian minerals up to March 1964. *Norges Geol. Undersøkelse,* **228,** 84–113.

BUGGE, J. A. W. (1943) Geological and petrographical investigations in the Kongsberg-Bamble formation. *Norges Geol. Undersøkelse,* **160,** 150 p.

CAMERON, E. N., R. H. JAHNS, A. H. MCNAIR, AND L. R. PAGE (1949) Internal structure of granite pegmatites. *Econ. Geol. Monogr.* **2,** 115 p.

CRUFT, E. F., C. O. INGAMELLS, AND J. MUYSSON (1965) Chemical analysis and the stoichiometry of apatite. *Geochim. Cosmochim. Acta,* **29,** 581–597.

DENISOV, A. P., O. B. DUDKIN, N. A. ELINA, R. A. KRAVCHENKO-BEREZHNOI, AND L. I. POLEZHAEVN (1961) Dependence of the physical properties of apatite on the admixture of rare earths and strontium. *Geokhimiya,* **8,** 666–675. [transl. *Geochem.* **8,** 718–730 (1961)].

Fersman, A. E. (1952) *Les Pegmatites. I. Les Pegmatites Granitiques.* Louvain et Bruxelles, 671 p.

FRONDEL, J. W. (1964) Variation of some rare earths in allanite. *Am. Mineral.* **49,** 1159–1177.

HAYNES, V. (1959) Compromise growth surfaces on pegmatite minerals. *Am. Mineral.* **44,** 1089–1098.

JAHNS, R. H. (1953) The genesis of pegmatites. I. Occurrence and origin of giant crystals. *Am. Mineral.* **38,** 563–598.

———, AND C. W. BURNHAM (1969) Experimental studies of pegmatite genesis. I. A model for the derivation and crystallization of granitic pegmatites. *Econ. Geol.* **64,** 843–864.

KHOMYAKOV, A. P. (1967) Chemical and crystallochemical factors in the distribution of rare earths. *Geokhimiya,* **2,** 197–205 [transl. *Geochem. Int.* **4,** 127–135 (1967)].

KORZHINSKIJ, D. S. (1965) *Abriss der Metasomatischen Prozesse.* Akademie-Verlag, Berlin, 195 p.

LAVES, F., AND K. SOLDATOS (1963) Die Albit-Mikroklin-Orientierungs-Beziehungen in Mikroklinperthiten und deren genetische Deutung. *Z. Kristallogr.* **118,** 69–102.

LINDBERG, M. L., AND B. INGRAM (1964) Rare earth silicatian apatite from the Adirondack Mountains, New York. *U.S. Geol. Surv. Prof. Pap.* **501-B,** B64–B65.

LYAKHOVICH, V. V. (1962) Rare-earth elements in the accessory minerals of granitoids. *Geokhimiya,* **1,** 37–52 [transl. *Geochem.* **1,** 37–55 (1962)].

MCKEOWN, F. A., AND H. KLEMIC (1957) Rare-earth-bearing apatite at Mineville, Essex County, New York. *Bull. U. S. Geol. Surv.* **1046-B,** 9–23.

MINEYEV, D. A. (1963) Geochemical differentiation of the rare earths. *Geokhimiya,* **12,** 1082–1100 [transl. *Geochem.* **12,** 1129–1149 (1963)].

OMORI, K., AND H. KONNO (1962) A new yttrian apatite enclosed in quartz from Naegi, Gifu Prefecture, Japan. *Am. Mineral.* **47,** 1191–1195.

PIGORINI, B., AND F. VENIALE (1968) L'apatite accessoria nella diverse facies litologiche delle formazioni granitoidi della Val Sersera (Vercelli). *Rendiconti Soc. Ital. Mineral. Petrol.,* **24,** 32 p.

RASS, I. T. (1964) Some rare elements in sphene and apatite of the Koksharov ultramafic-alcalic massif. *Geokhimiya,* **3,** 213–221. [trans. *Geochem. Int.* **2,** 230–241 (1964)].

RAST, N. (1965) Nucleation and growth of metamorphic minerals. In, W. S. Pitcher and G. W. Flinn, Eds., *Controls of Metamorphism.* Oliver and Boyd, Edinburg and London, p. 73–102.

SCHILLING, J. G., AND J. W. WINCHESTER (1967) Rare-earth fractionation and magmatic processes. In, S. K. Runcorn, Ed., *Mantles of the Earth and Terrestrial Planets.* Interscience Publishers, London-New York-Sidney, p. 267–283.

SCHNEIDERHÖHN, H. (1961) *Die Erzlagerstätten der Erde.* Vol. 2. *Die Pegmatite.* Gustav Fischer Verlag. Stuttgart, 720 p.

SEIFERT, H. (1953) Epitaxy. In, R. Gomer and C. S. Smith, Eds., *Structure and Properties of Solid Surfaces.* The University of Chicago Press, p. 318–383.

SHANNON, R. D., AND C. T. PREWITT (1969) Effective crystal radii in oxides and fluorides. *Acta Crystallogr.* **B25,** 925–946.

TABORSZKY, F. K. (1962) Geochemie des Apatite in Tiefengestein am Beispiel des Odenwaldes. *Beitr. Mineral. Petrogr.* **8,** 354–392.

TRÖGER, W. E. (1959) *Optische Bestimmung der Gesteinbildenden Minerale.* Teil **1.** *Bestimmungstabellen.* **3.** *Auflage.* E. Schweizerbart'sche Verlagsbuchhandlung, Stuttgart.

YERMAKOV, N. P. (1964) State and activity of fluids in chambered granitic pegmatites. *Int. Geol. Congress, Rep. 22nd Session. Part VI. Proc. Sect.* **6,** *Minerals and Genesis of Pegmatites.* New Dehli, p. 86–115.

YOUNG, E. J., AND E. L. MUNSON (1966) Fluor-chlor-oxy apatite and sphene from Crystal Lode pegmatite, near Eagle, Colorado. *Am. Mineral.* **51,** 1476–1493.

——— A. T. MYERS, E. L. MUNSON, AND N. M. CONKLIN (1969) Mineralogy and geochemistry of fluorapatite from Cerro de Mercado, Durango, Mexico. *U.S. Geol. Surv. Prof. Pap.* **650-D.**

ZIEBOLD, T. O., AND R. E. OGILVIE (1964) An empirical method for electron microanalysis. *Anal. Chem.* **36,** 322–327.

Manuscript received, April 26, 1974; accepted for publication, February 5, 1975.